© Photos: DOI: 10.2516/ogst/2013139, IFPEN, X

Dossier

This paper is a part of the hereunder thematic dossier published in OGST Journal, Vol. 69, No. 1, pp. 3-188 and available online here

Cet article fait partie du dossier thématique ci-dessous publié dans la revue OGST, Vol. 69, n°1, pp. 3-188 et téléchargeable ici

DOSSIER Edited by/Sous la direction de : **C. Angelberger**

IFP Energies nouvelles International Conference / Les Rencontres Scientifiques d'IFP Energies nouvelles

LES4ICE 2012 - Large Eddy Simulation for Internal Combustion Engine Flows

LES4ICE 2012 - La simulation aux grandes échelles pour les écoulements dans les moteurs à combustion interne

Oil & Gas Science and Technology – Rev. IFP Energies nouvelles, Vol. 69 (2014), No. 1, pp. 3-188

3> Editorial

11> *Boundary Conditions and SGS Models for LES of Wall-Bounded Separated Flows: An Application to Engine-Like Geometries*
Conditions aux limites et modèles SGS pour les simulations LES d'écoulements séparés délimités par des parois : une application aux géométries de type moteur
F. Piscaglia, A. Montorfano, A. Onorati and F. Brusiani

29> *LES of Gas Exchange in IC Engines*
LES échanges gazeux pour moteurs à combustion interne
V. Mittal, S. Kang, E. Doran, D. Cook and H. Pitsch

41> *Evaluating Large-Eddy Simulation (LES) and High-Speed Particle Image Velocimetry (PIV) with Phase-Invariant Proper Orthogonal Decomposition (POD)*
Évaluation de données de simulation aux grandes échelles (LES) et de vélocimétrie par imagerie de particules (PIV) via une décomposition orthogonale aux valeurs propres invariante en phase (POD)
P. Abraham, K. Liu, D. Haworth, D. Reuss and V. Sick

61> *Large Eddy Simulation (LES) for IC Engine Flows*
Simulations des grandes échelles et écoulements dans les moteurs à combustion interne
T.-W. Kuo, X. Yang, V. Gopalakrishnan and Z. Chen

83> *Numerical Methods and Turbulence Modeling for LES of Piston Engines: Impact on Flow Motion and Combustion*
Méthodes numériques et modèles de turbulence pour la LES de moteurs à pistons : impact sur l'aérodynamique et la combustion
A. Misdariis, A. Robert, O. Vermorel, S. Richard and T. Poinsot

107> *Investigation of Boundary Condition and Field Distribution Effects on the Cycle-to-Cycle Variability of a Turbocharged GDI Engine Using LES*
Études des effets des conditions aux limites et de la distribution des champs sur la variabilité cycle-à-cycle dans un moteur GDI turbocompressé en utilisant la LES
S. Fontanesi, S. Paltrinieri, A. D'Adamo and S. Duranti

129> *Application of LES for Analysis of Unsteady Effects on Combustion Processes and Misfi res in DISI Engine*
Application de simulation aux grandes échelles pour l'analyse des effets instationnaires de combustion et d'allumage raté dans les moteurs DISI
D. Goryntsev, K. Nishad, A. Sadiki and J. Janicka

141> *Eulerian – Eulerian Large Eddy Simulations Applied to Non-Reactive Transient Diesel Sprays*
Évaluation de la méthode Euler – Euler pour la simulation aux grandes échelles de sprays Diesel instationnaires non-réactifs
A. Robert, L. Martinez, J. Tillou and S. Richard

155> *Large-Eddy Simulation of Diesel Spray Combustion with Exhaust Gas Recirculation*
Simulation aux grandes échelles de la combustion d'un spray Diesel pour différents taux d'EGR
J. Tillou, J.-B. Michel, C. Angelberger, C. Bekdemir and D. Veynante

167> *Modeling of EGR Mixing in an Engine Intake Manifold Using LES*
Modélisation du mélange de EGR dans la tubulure d'admission à l'aide de la technique de LES
A. Sakowitz, S. Reifarth, M. Mihaescu and L. Fuchs

177> *LES of the Exhaust Flow in a Heavy-Duty Engine*
LES de l'écoulement d'échappement dans un moteur de camion
O. Bodin, Y. Wang, M. Mihaescu and L. Fuchs

Oil & Gas Science and Technology – Rev. IFP Energies nouvelles, Vol. 69 (2014), No. 1, pp. 177-188

DOI: 10.2516/ogst/2013117

IFP Energies nouvelles International Conference
Rencontres Scientifiques d'IFP Energies nouvelles

LES4ICE 2012 - Large Eddy Simulation for Internal Combustion Engine Flows
LES4ICE 2012 - La simulation aux grandes échelles pour les écoulements dans les moteurs à combustion interne

LES of the Exhaust Flow in a Heavy-Duty Engine

O. Bodin[1,2]*, Y. Wang[2], M. Mihaescu[1,2] and L. Fuchs[1,2]

[1] *CCGEx, KTH Mechanics, 100 44 Stockholm - Sweden*
[2] *Linné Flow Centre, KTH Mechanics, 100 44 Stockholm - Sweden*
e-mail: bodin@mech.kth.se - yue@mech.kth.se - mihai@mech.kth.se - lf@mech.kth.se

* Corresponding author

Résumé — **LES de l'écoulement d'échappement dans un moteur de camion** — L'écoulement dans l'orifice d'échappement et le collecteur d'échappement d'un moteur Diesel poids-lourd a été étudié en utilisant l'approche de simulation des grandes échelles (LES, *Large Eddy Simulation*). Quelques-unes des caractéristiques de l'écoulement de ces composantes sont : l'instabilité de débit et la séparation associée à la géométrie induite par le mouvement de flux secondaire. Une analyse détaillée de ces fonctions peut aider la compréhension et être utilisée pour diminuer les pertes de débit et accroître l'efficacité des composants en aval tels que les turbocompresseurs et les refroidisseurs EGR (*Exhaust Gas Recirculation*). Peu d'études LES de l'écoulement dans ces composants ont été menées dans le passé ce qui avec la complexité de l'écoulement motive ce travail. Cet article montre que, dans l'orifice d'échappement, même les paramètres globaux, comme les pertes de pression totale sont mieux traités par les LES que par les RANS (*Reynolds Averaged Navier Stokes*). Les structures d'écoulement qui affectent les performances de turbine et de l'efficience refroidisseur EGR sont générées dans le collecteur, celles-ci varient de façon significative pendant l'impulsion d'échappement. Ce document illustre aussi clairement la nécessité de faire des simulations couplées afin de traiter les conditions aux limites complexes de ces éléments d'échange de gaz.

Abstract *— **LES of the Exhaust Flow in a Heavy-Duty Engine** — The flow in the exhaust port and the exhaust manifold of a heavy-duty Diesel engine has been studied using the Large Eddy Simulation (LES) approach. Some of the flow characteristics in these components are: flow unsteadiness and separation combined with significant geometry-induced secondary flow motion. Detailed analysis of these features may add understanding which can be used to decrease the flow losses and increase the efficiency of downstream components such as turbochargers and EGR coolers. Few LES studies of the flow in these components have been conducted in the past and this, together with the complexity of the flow are the motivations for this work. This paper shows that in the exhaust port, even global parameters like total pressure losses are handled better by LES than RANS (Reynolds Averaged Navier Stokes). Flow structures of the type that affect both turbine performance and EGR cooler efficiency are generated in the manifold and these are found to vary significantly during the exhaust pulse. This paper also clearly illustrates the need to make coupled simulations in order to handle the complicated boundary conditions of these gas exchange components.*

INTRODUCTION

Modern heavy-duty Diesel engines use EGR and turbocharging to increase efficiency and reduce emissions. The subject of this study is the flow in an exhaust manifold and exhaust port of a six-cylinder heavy duty Diesel engine.

It has been shown by several researchers that the efficiency of the turbocharger is dependent on the flow structures at the turbine inlet, see for example Ehrlich *et al.* [1] and Hellström and Fuchs [2]. Even a simple pipe bend will generate significant secondary flow motion [3] and, as both the manifold and the exhaust port contain complex pipe shapes with bends and curvatures, strong and unsteady secondary flows will be generated.

Flow losses in the valve ports have a major impact on the efficiency of the gas exchange. The flow in intake ports has been studied in detail, by for example Gault *et al.* [4]. The character of the flow at the exhaust port is quite different compared to that at the intake port due to the differences in pressure gradients. When the exhaust valve opens, the pressure difference between cylinder and exhaust port is on the order of 500 kPa, with a temperature difference of more than 300 K.

In 1-D engine simulation tools such as for example GT-Power, one has to account for the complex 3-D flow by a discharge coefficient for the valve and valve port. Such model coefficients are usually obtained for stationary flows and at room temperature. Although the movement of the valve appears to have a smaller effect on the discharge coefficient, it is not clear if the discharge coefficient obtained at low mass flows can be reliably used in engine-like conditions. Evaluating the discharge coefficient of the valve itself, without the port can possibly improve 1-D modeling by separating the two loss sources.

A significant problem in engine design is the heat transfer from the hot exhaust to the exhaust valves, port and manifold. Accurately predicting the heat transfer to and from these components is important for valve design, but also for the assessment of the performance of the turbine and EGR cooler. The heat transfer in simple geometries has been studied in some detail and several engineering correlations exist. When these correlations are directly applied in more complicated flows like valve ports and manifolds they tend to fail in predicting the heat flux correctly, cf. Caton and Heywood [5]. The reason behind the poor results is that the turbulent flow in these geometries is far from being fully developed or statistically stationary for which the models were calibrated. Caton and Heywood [5] found that, for an exhaust port, the contributions to heat transfer from large scale fluid motion indeed dominated over the near wall boundary layer. This means that, if one aims at predicting instantaneous heat transfer in this kind of flow by computational methods, the three-dimensional and time-dependent flow field must be computed by an appropriate method.

The purpose of this paper is to characterize the flow in an exhaust manifold and port of a heavy duty IC-engine. The flow is characterized with respect to the generation of structures which affect the efficiency of EGR coolers and the turbine and in terms of global parameters. Also, sources of flow losses and flow features related to heat transfer are investigated.

1 CASE DESCRIPTION

The compressible flow calculations were carried out for two separate cases, the manifold and the exhaust port. The reason for the separation is the difficulty associated with running large cases with moving geometries which are very demanding in terms of computational time. No transfer of flow results from the port to the manifold, or vice versa, was done in the scope of this paper. Both the considered geometries are from the same Scania heavy-duty Diesel engine, the D12.

1.1 The Exhaust Port

The exhaust port geometry consists of five parts, a cylinder, a complex port with two pipes conjunct at one end, two valves and a long exit pipe as shown in Figure 1. The exit pipe is 10 exhaust pipe diameters long.

1.2 The Exhaust Manifold

The geometry of the manifold is shown in Figure 2. Visible are the inlets to the turbine, in the negative

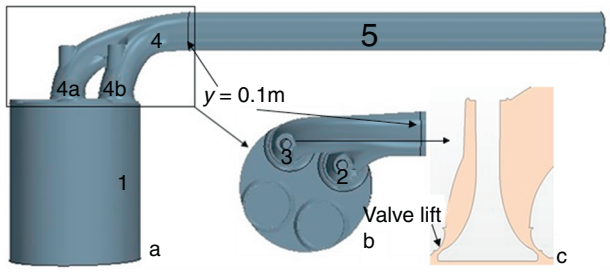

Figure 1

IC engine with only exhaust ports. a) The front view. b) The top view. c) The cross section of valve 3. 1) Cylinder. 2) Valve. 3) Valve. 4) Exhaust port. 5) Outlet domain.

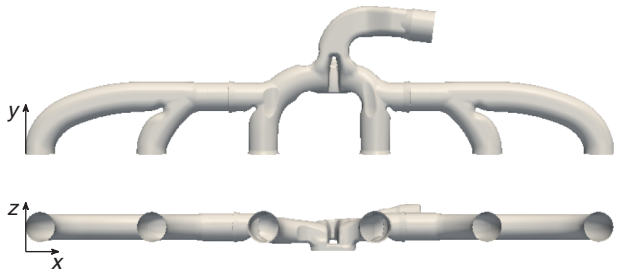

Figure 2

Manifold geometry and reference coordinate directions. Cylinders are numbered from the left.

z-direction, and to the EGR cooler. The cylinders will be referred to by the numbers 1 to 6 throughout this paper and the numbering goes from 1 to 6 in the positive x-direction. When referring to the pipes of the manifold, the word runner will be used so that runner 1 means the pipe connected to cylinder 1, runner 1 + 2 the piping connecting cylinders 1 and 2 to the manifold and so on. Clearly visible in Figure 2 is the asymmetry of this manifold. Runners 1 + 2 and 5 + 6 are mirror images but the central part with runners 3 and 4 as well as the two outlets do not have a symmetry plane. The computations do not take advantage of the geometrical symmetry since the flow itself is not symmetric.

1.2.1 Exhaust Port Boundary Conditions

The boundary conditions are chosen to match those of the experimental investigation carried out using the same geometry. A constant mass flow of 0.09 kg/s is applied at the bottom of the cylinder liner. The two valves are fixed at 4 mm valve lift. The outlet is kept at normal room conditions in accordance with the experiments and the wall boundary conditions are assumed to be no-slip velocity and adiabatic walls.

1.2.2 Manifold Boundary Conditions

The boundary conditions of computational cases are detailed in Table 1. Boundary conditions are of two categories: Engine-like pulsating flow through all six runners and steady flow through one inlet runner. As the name implies, engine-like conditions are obtained from a 1D simulation tool assuming hot, pulsating flow. An example of the inlet condition for the engine-like cases can be seen in Figure 3.

The major mass flow pulses such as the one located at 120° are the sum of the blowdown pulse from one side of the manifold, which for this example is runner 2, and the scavenging pulse from the other side, from runner 6. The blowdown pulse has a double-peaked appearance, probably because of pulse interaction in the manifold. The second pulse in the total mass flow, for example located at 140° are caused by the second peak in the scavenging pulse. If the scavenging pulse did not have two peaks, the total mass flow would probably not display two distinct peaks but rather have only one.

The manifold and the ports are constructed from cast iron, a material which is non-smooth. In fully developed flow conditions where the velocity profiles close to the wall are known, it is plausible to model the effect of wall roughness within LES but for the unsteady conditions such as the ones considered here, it is not. Because of the complicated geometry, the flow will never attain a fully developed profile.

The main effects of surface roughness are increased flow losses, laminar/turbulent transition and flow separation delay are all connected to the increased momentum mixing introduced by the roughness. These effects are not unimportant but, in order to take them into account fully, one would need to resolve the roughness and this is not possible due to the associated computational cost.

Because of this, the wall boundary conditions are no-slip walls, as for a smooth boundary with either adiabatic or isothermal condition, depending on the case. For numerical stability, the actual inlet and outlet boundaries are placed at extended location (*Fig. 4*), in

TABLE 1

Manifold case description

Case	BC type	Inlet mass flow (mean, max) (kg/s)	Wall	Inlet temp. (mean, max) (K)	Grid
M1	Steady	0.2, -	Isothermal (600 K)	790, -	1
M2	Steady	0.2, -	Isothermal (600 K)	790, -	2
M3	Steady	0.2, -	Isothermal (600 K)	790, -	3
M4	1 900 rpm	0.11, 0.48	Isothermal (600 K)	786, 978	3

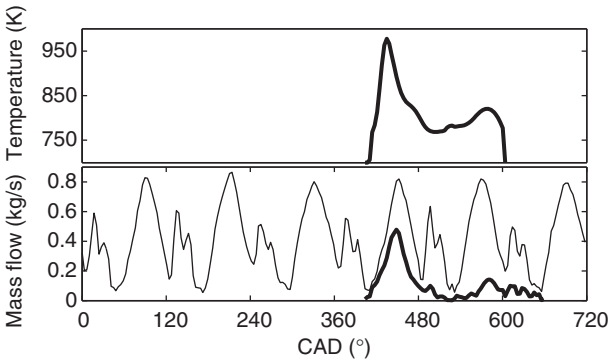

Figure 3

Phase averaged inlet mass flow and temperature from Case 4. '–' (thick line), mass flow and temperature from runner 1, '–' (thin line), mass flow from all runners.

Figure 4

Added volumes for computational stability in dark grey.

order to reduce the uncertainty in boundary condition. In these added regions, because their purpose is strictly numerical, the slip boundary condition is applied at the walls.

1.3 Computational Grids

In the exhaust port, the grid is completely hexahedral. Cell size and shape vary throughout the computational domain. In the valve gap, the cells are highly isotropic with a 0.07 mm side which, compared to the valve lift (4 mm), implies that the relative cell size is $0.07/4 = 0.0175$. In the rest of the domain and particularly in the outlet domain (*e.g.* Part 5 in *Fig. 1*) the grid is stretched in the flow direction.

For the exhaust manifold, the grids used are mostly isotropic with hexahedral cells and some polyhedra close to the walls. No grid stretching was used in the manifold domain (light grey in *Fig. 4*). Quite aggressive grid stretching was used in the two outlet domains (dark grey in *Fig. 4*) in order to damp the reflections from the outlets. Three different grid resolutions were used during the investigation, called grid 1, 2 and 3 with a cell size of 1, 0.8 and 0.6 mm respectively. These cell sizes correspond to a relative cell size of 0.023, 0.019 and 0.014 respectively when the diameter of the circular inlets to the manifold (43 mm) is used as reference.

2 NUMERICAL METHOD

Two numerical codes were used in this investigation, StarCCM+ [6] and EDGE [7]. The reasons for using two separate codes are the mesh movement capabilities of StarCCM+ and the efficiency of EDGE.

StarCCM+ is a compressible flow solver with second order implicit time-stepping and a bounded central-difference (BSD) scheme (which can be generally described as a scheme mixing a first-order upwind scheme, a second-order upwind scheme and a central-differencing scheme) for space discretization. A second order upwind convection scheme has been used in for the RANS (Reynold Average Navier Stokes) simulation in StarCCM+. All exhaust port calculations were carried out using StarCCM+.

The EDGE code is a compressible edge-based finite volume solver with a four-stage, second order Runge-Kutta time stepping. Spatial discretization is a formally second order central scheme with Jamesson-type artificial dissipation. All exhaust manifold calculations were carried out using EDGE.

2.1 Turbulence Modeling

2.1.1 RANS

For all RANS calculations, the standard k-ε model was used together with classical wall functions, see for example [8]. The reasons for using this approach are that this is commonly used by the industry and there is a need to compare the results of RANS and LES, also for mean and rms of the variables. In the context of this paper, RANS calculations were carried out for the port geometry only.

2.1.2 LES

For all LES calculations no explicit, Sub-Grid-Scale (SGS) model is used. This approach uses the inherent numerical dissipation to account for the effect of the unresolved subgrid dissipation. It has been used by many

researchers for a number of years and in many applications, see for example [9] and [10]. However, without an explicit SGS model, the simulations must have adequate resolution. The SGS terms are the result of the filtering of the non-linear terms:

$$\frac{\partial u}{\partial t}+\frac{\partial F(u,x)}{\partial x}=0 \tag{1}$$

The filtering operation introduces the subgrid scale term, called *SGS* below, to the equation which now is for the filtered variable $\overline{u}$:

$$\frac{\partial \overline{u}}{\partial t}+\frac{\partial \overline{F(\overline{u},x)}}{\partial x}=\frac{\partial \overline{F(\overline{u},x)}}{\partial x}-\frac{\partial F(u,x)}{\partial x}=SGS \tag{2}$$

The right hand side of Equation (2) is the SGS term. When this equation is discretized, another rest term is introduced which contains the truncation errors, T associated with the particular scheme used:

$$\frac{\partial \overline{u}}{\partial t}+\frac{\partial \overline{F(\overline{u},x)}}{\partial x}=SGS+T \tag{3}$$

The *SGS* term must, in order for the LES to produce reasonable results, account for the behavior of the fluid scales that it filters away. If the filter width is small enough, the scales that are filtered away have an isotropic and problem independent (*i.e.* universal) nature and are mostly responsible for dissipation of kinetic energy into heat.

One motivation for implicit LES is that this dissipative nature is something which these scales share with stable numerical schemes and, since the effect of the *SGS* and T terms are additive, their total effect may be accounted for by the numerical scheme, T. Of course, this approach makes the dissipation completely dependent on the grid and the numerical scheme, both of which are non-physical. The benefits of this approach are simplicity and speed since no *SGS* model is used and also that there is no unwanted dissipation present.

3 METHOD VERIFICATION

With the LES method used (see *Sect. 2.1.2*), because of the implicit filtering, grid independent results is only strictly possible in the DNS limit. Investigating that limit is not practical. However, we analyze the sensitivity of the results to grid resolution for the exhaust manifold case. In Figure 5, the mean axial velocity from two perpendicular lines is plotted. These two lines are located in Plane 4 as shown in Figure 6. The coordinate used in

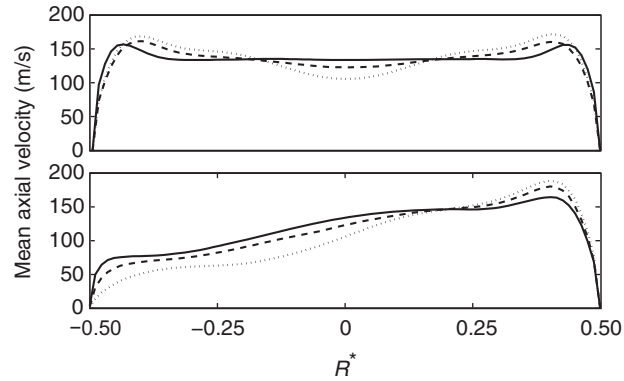

Figure 5

Sensitivity to grid resolution in the manifold, mean axial velocity *versus* R^*. Lines are located on plane 4 (see *Fig. 6*) and are directed in the y direction (bottom figure) and in the z direction. Grid 1, '...' (Case M1, coarsest). Grid 2, '- -' (Case M2). Grid 3 '–' (Case M3, finest).

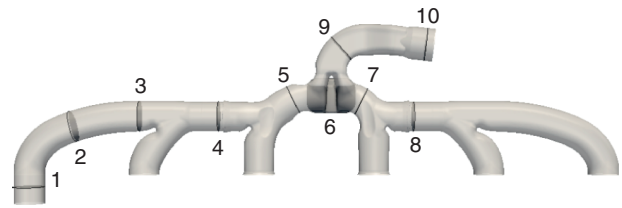

Figure 6

Manifold sample planes with corresponding numbers.

Figure 5, the equivalent radius R^*, is the radius of a circle with an area equal to the plane in question, in this case plane 4 (see *Fig. 6*). As expected, the solution has not reached grid-independence but, with the grids tested, does have a monotonic convergence. The absolute deviation:

$$\Delta_k=\sqrt{(q_{n,k}-q_{m,k})^2} \tag{4}$$

can be used to quantify the differences between the solutions. One may use Equation (4), where $q_{n,k}$ and $q_{m,k}$ are the investigated property at the point k from Grid n and m respectively, and calculate the average absolute deviation between the grids. This is done by taking the arithmetic average of Δ_k and then dividing by the arithmetic average of $q_{n,k}$ over all points k under consideration. Doing this gives that the mean deviation between Grid 1 and 2 is about 12%, while between 2 and 3 the deviation is approximately 7.5%.

To further analyze the deviations, the variance over k of Δ_k was calculated and gave for the deviation between grid 1 and 2 a value of about 88%, while for the 2 and 3 deviation, the variance is approximately 29%. The result is made non-dimensional in the same way as for the average absolute deviation above.

Taken together, monotonic convergence, decrease in both average absolute deviation and variance as well as a average absolute deviation of 7.5% between Grids 2 and 3 means that Grid 3 is adequately fine for the purpose of this paper.

A post-*priori* way of checking if the grids used are adequately fine can be performed using the Power Spectral Density (PSD) of the velocity fluctuations. Although the flow in neither manifold nor port can be considered fully developed turbulent, some characteristics of fully developed turbulence are expected also here.

These characteristics include the turbulent cascade, where energy is transported from large scales to the small ones and finally dissipated into heat. LES should resolve a significant part of the so called inertial range of these scales where the power of velocity fluctuations in isotropic turbulence depend on the frequency, f, like $f^{-5/3}$.

The Power Spectral Density (PSD) of the axial velocity component at the center of plane 4 (*Fig. 6*) for cases 3 and 4 are plotted in Figure 7.

The range of frequencies in the inertial range for both steady and pulsating flow appears to be at least one order of magnitude and this is deemed sufficient. In the port, the PSD of the axial velocity component at the location $y = 0.1$ in Figure 1 is plotted in Figure 8. For the port calculations, the resolution seems to be adequate as well, with about one order of magnitude frequencies contained within the inertial range.

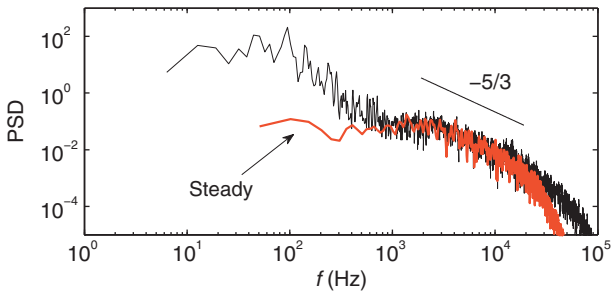

Figure 7

Power spectral density of axial velocity component at the center of plane 4 in the manifold (see *Fig. 6*) for steady inflow through runner 1 and 1 900 rpm engine-like conditions. Additional line has the −5/3 slope associated with the inertial range of scales in isotropic turbulence.

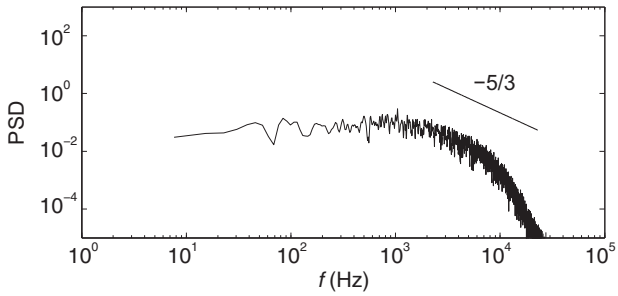

Figure 8

Power spectral density of axial velocity component at the center of a plane at $y = 0.1$ in Figure 1 in the port. Additional line has the −5/3 slope associated with the inertial range of scales in isotropic turbulence.

4 RESULTS

4.1 Exhaust Port Flow

RANS results are included in this paper in order to make a comparison between what is widely used in the vehicle industry and the present LES. The turbulence model chosen is the standard k-ε model with classical wall functions. As compared to RANS, LES has much higher potential for accurately predicting the flows in gas exchange components like the manifold and port.

Not only that LES is able to handle the unsteady time-resolved flow but the prediction of time averaged quantities like the total pressure loss will also be improved as compared to RANS. In Table 2, a comparison between the experiment, RANS and LES total pressure drop in the exhaust port is given.

Clearly, LES predicts the pressure drop much closer to the experimental results. Given the nature of the flow in the port, with separation and stagnation regions, this is not unexpected. Many of the assumptions in the k-ε model and the wall functions are simply to severe for the flow in an exhaust port.

The flow in the exhaust port is highly unsteady and characterized by the narrow valve gap through which the fluid is forced as shown in Figure 9. When the flow comes out of the cylinder through the valve gap, it is first accelerated due to the reduction in cross-sectional area of the flow path and then decelerated in to the exhaust port, where the cross-sectional area increases. Due to the presence of the valve an annular, jet-like flow structure is formed where the high-velocity flow follows the valve stem into the port where it curves along the outer bend.

TABLE 2
Results of experiments *vs* RANS *vs* LES

	Experiment	RANS	LES
Total pressure drop (kPa)	4.9	5.4	5.0
The difference compared to experiment (kPa)	-	0.50	0.10
The difference compared to experiment (%)	-	10	2

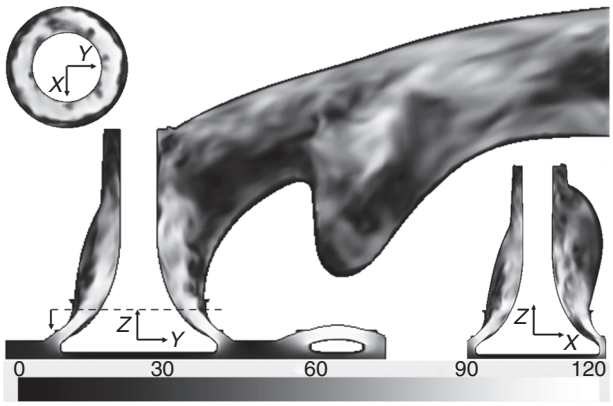

Figure 9
Instantaneous velocity magnitude of LES simulation in the port.

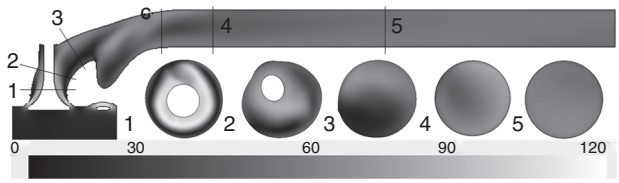

Figure 10
Mean velocity magnitude of LES simulation in the port.

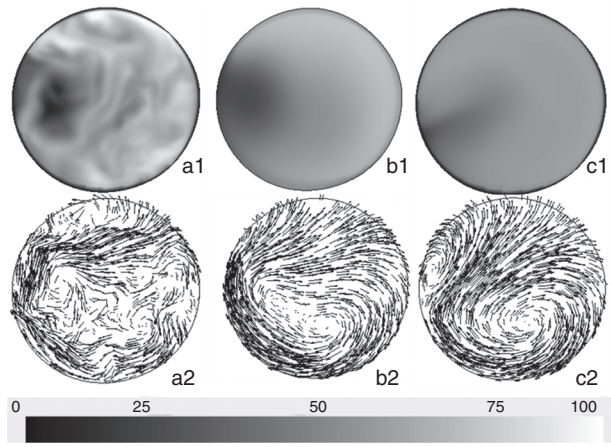

Figure 11
Velocity field in the cross section of junction (Plane C in *Fig. 10*), from left to right are: a) instantaneous velocity of LES; b) mean velocity of LES; c) RANS velocity field.

There is flow separation immediately downstream of the valve seat on the walls of the port and also on the surface of the valve body. These flow features can also be seen in the mean velocity field distribution of Planes 1 to 3 shown in Figure 10.

The port contains two valves and two valve-channels that are joined downstream (*Fig. 1*) but, as the flow has similar characteristics in both, only one is shown and analyzed here. Because the high-speed flow follows the valve stem, there is no significant wake downstream of the stem. This is evident both in the instantaneous (*Fig. 9*) and average data (*Fig. 10*).

A comparison between instantaneous LES, mean LES and RANS axial velocity (at the location C in *Fig. 10*) can be seen in Figure 11. This particular position is where the manifold would be joined to the port so it represents possible inlet conditions for the manifold.

The differences among the cases are relatively small, both for the axial component and the in-plane structures. Both of the mean in-plane plots exhibit a rather large clockwise rotating vortex in the lower half on the plane. In the RANS data there is also a second, counter-rotating, vortex in the upper part of the plane which is not present in the LES data. The instantaneous LES flow field shows a multitude of small structures in both the in-plane, and axial velocity data which indicate that the vortex in the mean velocity field is probably not a coherent structure.

The conditions at the plane in Figure 10 represent the flow generated by the port geometry. This is interesting in itself but also because it represents the inflow into the exhaust manifold. The manifold calculations presented here have uniform plug flow inlet conditions which are, as seen in Figure 10, not a good representation of the true conditions. These boundary conditions are to be used for comparison with more realistic ones in the future. The authors also believe the studying the flow in the manifold using simplified boundary conditions can provide an useful insight which is valid also with more realistic boundary conditions.

4.2 Steady Boundary Condition Manifold Flow

One of the motivations for this paper is the importance of the inflow conditions to the turbocharger turbine. However, because of the complicated geometry, the analysis is not straightforward. In order to reduce the data, the flow uniformity index, γ is defined.

$$\gamma = 1 - \frac{1}{2\overline{q}A}\sum_{i=1}^{n}\sqrt{(q_i - \overline{q})^2}A_i \qquad (5)$$

The plane in question is divided into n parts, each with a corresponding q_i which represents the investigated variable. The total area of the plane is A and $\overline{q}$ is the area average of q. This method is used as a way of representing the non-uniformity of the flow in a plane. In Figure 12, the mean axial velocity is plotted in the manifold together with the uniformity index of the mean axial velocity for case M3. The location of the investigated planes can be observed in Figure 6.

At the first plane the uniformity index is quite high and the axial velocity does not vary much over the plane. Plane 1 is located in a part of the computational domain which has parallel walls and a slip wall boundary condition, see Figures 4 and 6.

Moving on to the second plane, there is a clear effect of the curved shape of the geometry which results in the fluid at the inner bend separating. Also, the fluid close to the walls shows evidence of a strongly accelerated boundary layer which is expected due to the close proximity to the plug-flow inlet.

When a time-dependent plug-flow inlet encounters the no-slip wall there will be a strong deceleration of the boundary layer which result in a velocity profile maximum quite close to the wall. The reason for this is that the fluid in the central parts of the flow is associated with a larger amount of inertia and will thus react more slowly. This, together with the conservation of mass, and the no-slip condition, will give the type of flow observed.

The uniformity index is reduced slightly in the second plane, most likely because of the separation zone.

The third plane actually increases the uniformity index, not only compared to Plane 2 but also compared to Plane 1. At the third plane, curvature has decreased and the effect on the flow is less pronounced than at Plane 2. There is evidence of the accelerated boundary layer just as the preceding planes.

The fourth plane is located in runner 1 + 2 so is downstream of the (for this case) cavity that is runner 2. Here, the flow field has many similarities with Plane 3 and no clear evidence of any effect of runner 2 can be seen.

At the fifth plane, the axial flow field exhibits a separation on the left side due to a kink in the manifold. This separation pushes the flow to the right side of the pipe.

The most prominent long-lived features are the flow separations due to the pipe geometry and the not fully

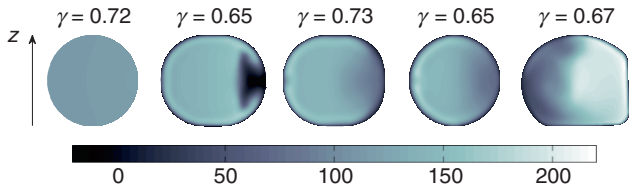

Figure 12

Case M3. Mean axial velocity of, from left to right, Planes 1 to 5 (see *Fig. 6*) and the corresponding uniformity index in the exhaust manifold.

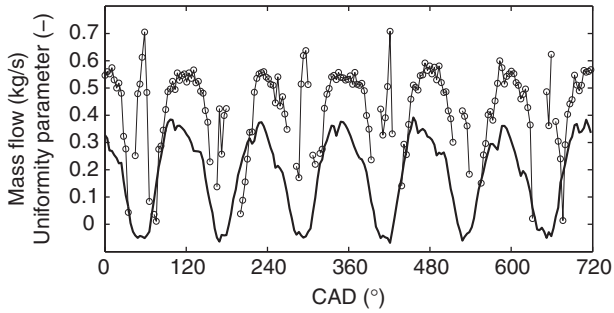

Figure 13

Phase averaged mass flow '-' and flow uniformity index (γ), o' at the turbine inlet plane for 1 900 rpm, Case M4.

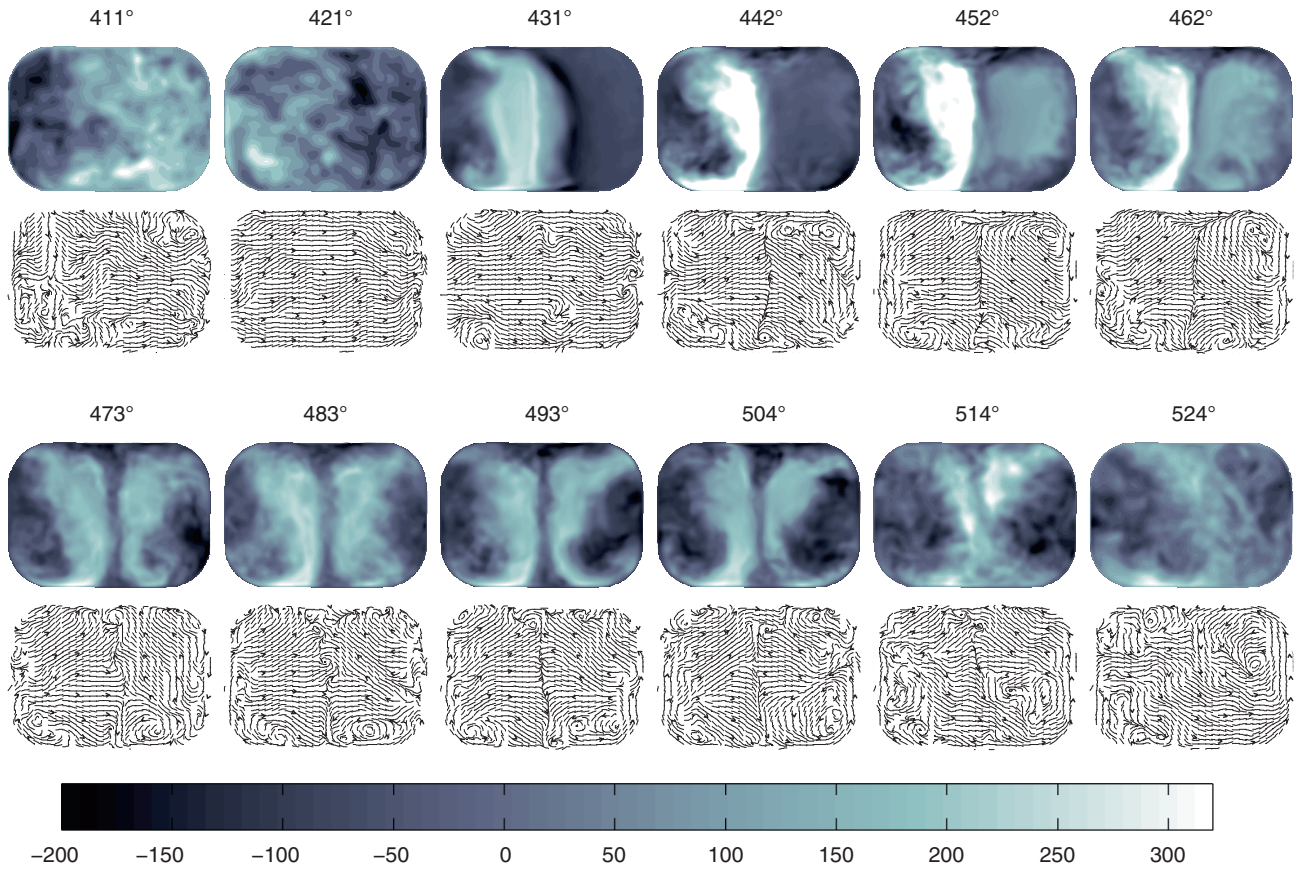

Figure 14

Phase average axial momentum at turbine inlet plane and in-plane flow structures. Runners 1-3 is on the left and flow is directed into figure.

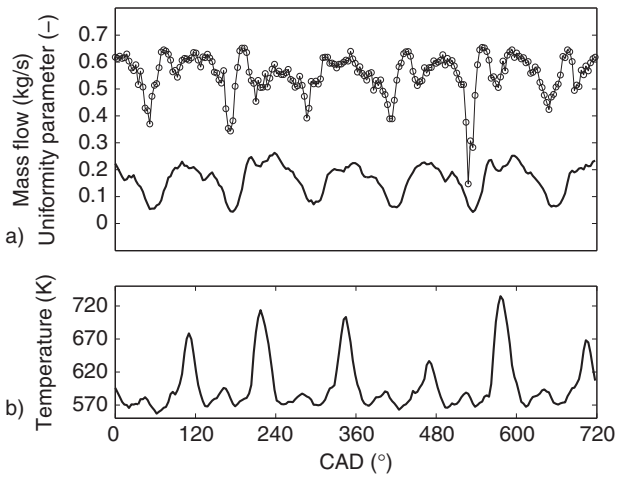

Figure 15

a) Phase averaged mass flow '-' and flow uniformity index (γ), 'o' at the EGR cooler inlet plane for Case M4. Horizontal arrow shows the exhaust period of cylinder 1. b) Phase averaged mean temperature at EGR inlet plane.

developed boundary layers. Since the inlet flow contains no secondary flow nor turbulent fluctuations all such features are generated by the flow itself. The generation of such features is associated with a loss of the available energy at the inlet which, for steady flow, is straightforward to assess.

From inlet to Plane 5, the flow loses about 5% of the total pressure where the majority of these losses occur between Planes 4 and 5.

4.3 Unsteady Boundary Condition Manifold Flow

The flow data with steady boundary condition is useful for giving some insight into the geometry-induced flow features. However, the manifold is designed for, and operates in, pulsating flow involving all the runners. This means that if one strives at investigating the conditions at EGR cooler and turbine inlet, engine-like boundary conditions and phase averaging are necessary. Because of the significant time requirements necessary to obtain

phase average LES data, only 5 cycles (5×720 crank angle degrees) are used.

In order to analyze the flow at the turbine inlet plane, the phase average mass flow and flow uniformity index, Equation (5), is calculated. In Figure 13, this data is presented as a function of crank angle. The flow uniformity index is edited so that no negative values are shown. A negative γ value is possible numerically when the averaged axial flow velocity is very small making the second term in Equation (5) larger than 1 and γ smaller than 1. This can only happen at very low mass flows, where the turbine is not producing any power and the inflow condition is irrelevant for turbine performance.

The general behavior of γ is that it has two peaks for each mass flow pulse, one during the initial acceleration when the mass flow is low and one, with a much longer duration, which coincide with the mass flow pulse itself. The short duration peak is probably present because of the stabilizing effect of acceleration and the low flow velocity which combines to produce the high value of γ. However, as the mass flow is low, this part of the flow is rather insignificant when turbine performance is concerned.

The really interesting part for turbine performance is when the mass flow is high and then γ has a value between 0.5 and 0.6. Computing the flow uniformity index gives only a rough idea about the conditions at the turbine inlet plane and to further understand the flow, the axial momentum and in-plane flow structure during a mass flow pulse is visualized in Figure 14 for the turbine inlet plane.

During the acceleration phase, the flow field is highly skewed because of the blowdown pulse coming from runner 1 which is coming from the figure left. When the maximum mass flow is approached, the scavenging pulse of runner 4, which is on the right, contributes to

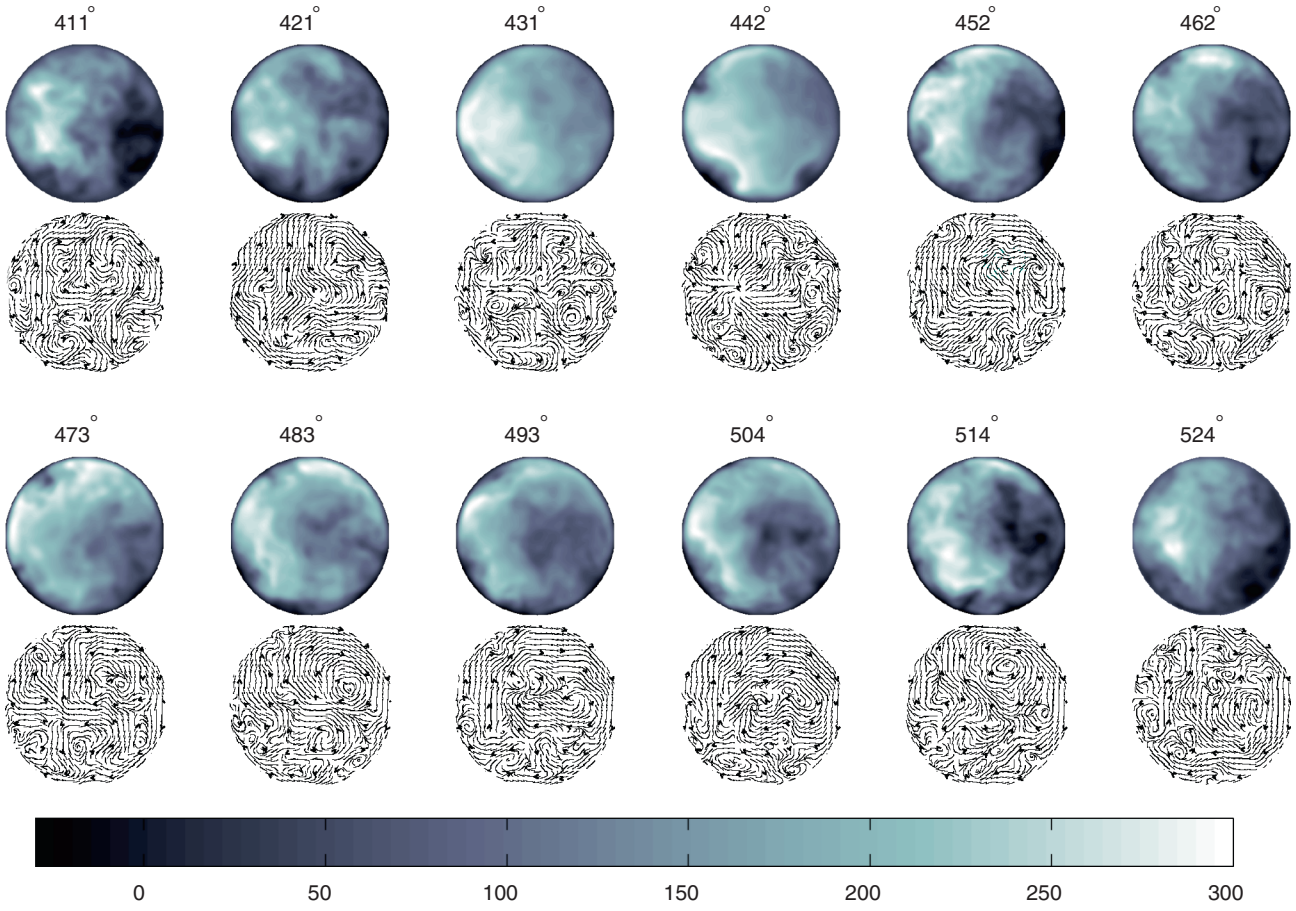

Figure 16

Phase average axial momentum at EGR cooler inlet plane and in-plane flow structures. Inner radius is on the right side and the axial flow is directed into the figure.

the total mass flow and makes the flow more evenly distributed. For this particular pulse, the maximum γ is reached after the maximum mass flow close to 483°. The secondary flow structure shows clear evidence of a strong shear layer in the middle of the turbine inlet plane which is particularly apparent during the blowdown phase of runner 1 at 442°.

Other in-plane structures are quite small, vortex structures are apparent throughout the cycle but are not dominating the flow in any sense. At 483° where the mass flow is at maximum, vortices generated by geometry curvature are located by the edges of the inlet plane and the shear layer generated by the manifold division is not as strong as earlier in the cycle.

At the EGR cooler inlet plane, Figure 15, γ is generally slightly higher compared to the turbine inlet plane.

The reason is most likely that the flow here is not as strongly affected by the split design of the manifold as is the case with the turbine inlet plane.

Just like for the turbine inlet, the flow uniformity index increases rapidly during the initial part of flow acceleration but the short duration peaks of high γ is not present. When the mass flow decreases, γ follows it. In addition to flow uniformity and mass flow, the area average temperature is also plotted in Figure 15. The temperature peaks occur during the first half of the mass flow pulse where the main contribution to the mass flow pulse comes from a blowdown pulse.

In the same way as for the turbine inlet plane, the axial momentum and in-plane flow structure during a mass flow pulse is visualized in Figure 16 for the EGR cooler inlet plane.

The flow in the EGR cooler inlet plane is characterized by a higher axial momentum in the outer bend and many small diameter vortical structures in the in-plane velocity field. These vortices are much more dominating compared to the turbine inlet when mass flow, and cooling needs are high.

DISCUSSION AND CONCLUSIONS

Standard k-ε using classical wall functions are clearly unsuited to study the flow in the exhaust port, even for evaluation of averaged quantities like total pressure losses. The reason for this is the nature of the flow and the inherent assumptions of the models.

It is clear that relatively large scale, unsteady features dominate the flow in both the port and the manifold, even for stationary valves and steady boundary conditions. In the port, the velocity profiles are skewed so that the maximum is in the upper part of the port and quite large zones of separated flow are evident on the port walls. Because the flow are mostly parallel to it, no significant wake is produced by the interaction between the flow and the valve stem. If heat transfer is to be analyzed in the port, these features must be taken into account and this is clearly not within the scope of simple engineering models or simple RANS. The flow field at the port exit contains significant secondary flow structures which are likely to have an effect on the flow in the exhaust manifold.

The flow in the exhaust manifold is characterized by non-equilibrium boundary layer and of geometry-induced flow effects. Analysis of this kind of exhaust manifold must also take into account that it is constructed for pulsating flow where exhaust periods overlap.

The flow uniformity coefficient, γ, which is widely used to characterize internal flows is found to be useful in providing information on the variation of inflow conditions at the EGR cooler and turbine inlet planes.

Good qualitative agreement is found between the flow acceleration and increase in γ which agree with the general stabilizing effect of acceleration in fluid flow. At the turbine inlet, γ is typically slightly below 0.6 during the high mass flow part of the pulse. Visualization of the flow field at the inflow plane to the turbine shows a generally highly non-uniform axial distribution. In-plane flow structures include a clearly defined shear layer generated by the divided geometry and small vortices, probably generated by geometry curvature. Based on previous results, cf. Ehrlich *et al.* [1] and Hellström and Fuchs [2], the flow conditions generated in the manifold are such that they will have an effect on turbine performance.

At the EGR cooler inlet, the flow field is also non-uniform and shows higher flow velocities at the outer radius of the inlet channel curvature. During the high mass flow part of the pulse, gamma is generally around 0.6. Here, the inflow structures are made up of vortices located all over the inlet plane. The flow fields at both locations vary significantly during the exhaust period in a way not predictable by γ alone. Indeed, no one-valued function is likely to give an accurate description of complicated flow fields such as these.

The observations made in this paper give insight into the characteristics of the flow in the exhaust port and manifold. However, both cases are computed using simplified boundary conditions and it can not be said with certainty that the obtained results are representative for actual engine conditions. In order to gain insight into this, LES calculations using more realistic boundary conditions must be carried out. The conditions inside the cylinder when the exhaust valve opens and the valve movement is likely to have an effect on the flow field in

the exhaust port. This will in turn affect the flow field in the exhaust manifold. Finally, the turbocharger turbine and EGR cooler, which are situated at the exhaust manifold outlet will have an effect on the flow in the exhaust manifold.

ACKNOWLEDGMENTS

This work was financed by KTH CCGEx. The Swedish National Infrastructure for Computing (SNIC) has provided computational resources. Stefan Gundmalm and Martin Söder provided data used for boundary conditions. Martin Söder provided data on surface roughness and material properties of the manifold and, most importantly, the computational grids for the manifold used in this investigation. The Swedish defense research agency (FOI) provided the computational code used in the manifold simulations. All these contributions to this work are greatly appreciated.

REFERENCES

1 Ehrlich D.A., Lawless P.B., Fleeter S. (1997) On-engine turbocharger turbine inlet flow characterization. *48th Earthmoving Industry Conference & Exposition*, 9 Apil, Peoria, Illinois, SAE Technical Paper 971565.

2 Hellström F., Fuchs L. (2008) Effects of inlet conditions on the performance of a radial turbine. *53rd ASME Turbo Expo*, Berlin, 9-13 June, Paper no. 6T2008-51088, pp. 1985-2001.

3 Sudo K., Sumida M., Hibara H. (1998) Experimental investigation on turbulent flow in a circular-sectioned 90-degree bend, *Exp. Fluids* **25**, 1, 42-49.

4 Gault R.I., Thornhill D.J., Fleck R., Mackey D.O., Chatfield G.F. (2004) Analysis of the steady flow characteristics through a poppet valve, *SAE 2005 Trans. J. Eng.* **113**, 3, 1080-1093.

5 Caton J.A., Heywood J.B. (1981) An experimental and analytical study of heat transfer in an engine exhaust port, *Int. J. Heat Mass Trans.* **24**, 4, 581-595.

6 CD-Adapco. StarCCM + User Guide 6.06.017. Technical report, (2011) URL http://www.cd-adapco.com/.

7 Eliasson P. (2001) EDGE, a NavierStokes Solver for Unstructured Grids. Technical report, Scientific Report FOI-R–0298–SE, Computational Aerodynamics Department, Aeronautics Division, FOI.

8 Wilcox D.C. (2006) *Turbulence moddeling for CFD*. DCW Industries, 3rd ed, ISBN 1928729088, 9781928729082.

9 Grinstein F.F., Margolin L.G., Rider W.J. (2007) *Implicit Large Eddy Simulation: Computing Turbulent Fluid Dynamics*, Cambridge University Press, ISBN 052186982X.

10 Rutland C.J. (2011) Large-eddy simulations for internal combustion engines - a review, *Int. J. Engine Res.* **12** 5, 421-451, ISSN 1468-0874. doi: 10.1177/1468087411407248.

Manuscript accepted in Febuary 2013
Published online in October 2013